



Recent advances and applications of WRF–SFIRE

J. Mandel^{1,2}, S. Amram^{3,4}, J. D. Beezley⁵, G. Kelman^{3,6}, A. K. Kochanski⁷, V. Y. Kondratenko¹, B. H. Lynn^{3,6}, B. Regev^{3,4}, and M. Vejmelka^{1,2}

¹University of Colorado Denver, Denver, CO, USA

²Institute of Computer Science, Czech Academy of Sciences, Prague, Czech Republic

³The Hebrew University of Jerusalem, Jerusalem, Israel

⁴Ministry of Public Security, Jerusalem, Israel

⁵CERFACS and Météo France, Toulouse, France

⁶Weather It Is, LDT, Efrat, Israel

⁷University of Utah, Salt Lake City, UT, USA

Correspondence to: J. Mandel (jan.mandel@gmail.com)

Received: 20 December 2013 – Published in Nat. Hazards Earth Syst. Sci. Discuss.: 24 February 2014

Revised: 6 September 2014 – Accepted: 15 September 2014 – Published: 31 October 2014

Abstract. Coupled atmosphere–fire models can now generate forecasts in real time, owing to recent advances in computational capabilities. WRF–SFIRE consists of the Weather Research and Forecasting (WRF) model coupled with the fire-spread model SFIRE. This paper presents new developments, which were introduced as a response to the needs of the community interested in operational testing of WRF–SFIRE. These developments include a fuel-moisture model and a fuel-moisture-data-assimilation system based on the Remote Automated Weather Stations (RAWS) observations, allowing for fire simulations across landscapes and time scales of varying fuel-moisture conditions. The paper also describes the implementation of a coupling with the atmospheric chemistry and aerosol schemes in WRF–Chem, which allows for a simulation of smoke dispersion and effects of fires on air quality. There is also a data-assimilation method, which provides the capability of starting the fire simulations from an observed fire perimeter, instead of an ignition point. Finally, an example of operational deployment in Israel, utilizing some of the new visualization and data-management tools, is presented.

1 Introduction

Wildland fire is a complicated multiscale process. The fire behavior is affected by very small-scale thermal degradation processes occurring well before the flames appear at the molecular scale (Sullivan and Ball, 2012). Slightly larger-scale turbulent processes induce mixing of the combustible gasses with the ambient air, and transport of heat, moisture, and combustion products into the atmosphere, affecting the fire as well. See Sullivan (2009b, c, d) for a survey and a discussion of the complexity of the problem.

In a case of a wildland fire, all of these processes, no matter how small-scale, are affected to some degree by larger scale weather conditions. The energy from the large scales drives a cascade of gradually smaller and smaller eddies that generate local winds, driving wildland fire propagation. According to the Kolmogorov hypothesis, the energy content of the eddies that are responsible for small-scale mixing is controlled by larger-scale eddies, as the energy propagates from larger to smaller scales. Consequently, any mixing-limited chemical reaction in the atmosphere is ultimately affected by large-scale processes providing energy for turbulent mixing. Although chemical-reaction rate is affected by concentrations of reacting species, in the case of gas-phase oxidation, these concentrations are generally affected (or limited) by local mixing.

Large-scale weather patterns induce changes in temperature and humidity, which affect fuel moisture, thus affecting the fire behavior as well. Fire behavior is highly sensitive to fuel-moisture content (FMC), which affects the burning process in at least three ways (Nelson Jr., 2001): it delays ignition, decreases fuel consumption and increases particle residence time. By increasing fuel-moisture content, the spread rate decreases, and, eventually, at the extinction-moisture level, the fire does not propagate at all (Pyne et al., 1996). In Rothermel's spread-rate model, for example, fire-spread rate depends on the fuel-moisture ratio through an empirical moisture damping coefficient (Rothermel, 1972, Fig. 7) (see Fig. 1).

The fuel-moisture content depends on fuel properties and on atmospheric conditions. The fuel-moisture content of live fuels exhibits predominantly a seasonal variation driven by physiological regulatory processes. In contrast, the fuel-moisture content of dead fuels is influenced by a variety of weather phenomena, such as precipitation, relative humidity, temperature, wind conditions, dew formation, and even solar radiation. For a recent review on modeling processes affecting fuel moisture in dead fuels, see Matthews et al. (2010). Diurnal variations in the dead fuel moisture, often disregarded in simulations of short fires, become important in the case of prolonged fires. These fires stay active over periods of days or even weeks, over which fuel-moisture conditions can significantly change. Even though one can imagine particular meteorological conditions with negligible daily fluctuations in the temperature, relative humidity and, consequently, also the fuel moisture, nevertheless, diurnal variations in fuel-moisture content affect fire activity. For that reason, simulations of multi-day wildland fires, such as those presented in this study, require estimates (or forecasts) of moisture-content changes during the fire event.

Synoptic flows are affected by topography and land-use characteristics. If a fully physical representation of the wildland fire propagation was chosen, a wide range of scales would have to be modeled, from 10^{-4} m combustion processes to 10^5 m plume (Sullivan, 2009a) and planetary-scale (10^7 m) weather systems. Although treating a subset of the scales by direct numerical simulation is technically feasible to some degree for very small fires – e.g., Linn and Cunningham (2005); Mell et al. (2007) –, the massive computational costs of such simulations and amounts of time required make them prohibitive from an operational point of view. Fortunately, coupling of a mesoscale weather model with a 2-D fire-spread model captures a practically important range of wildland fire behavior (Clark et al., 1996a, b). Combustion and the heat transfer from the fire to unburned fuel are parameterized in the spread-rate calculation, and the wind speed affects the rate of fire spread; e.g., Rothermel (1972), Albini (1981, 1982) and Beer (1991). Conversely, the fire influences the weather through the heat and vapor fluxes from burning carbohydrates and evaporation. The buoyancy created by the heat from the fire can cause intense updrafts,

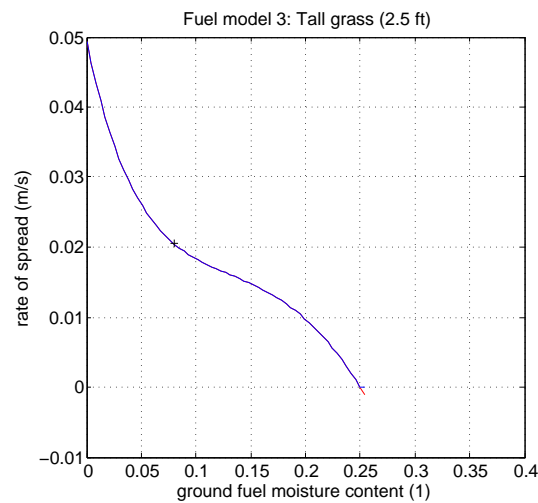


Figure 1. Illustration of the dependence of rate of spread on fuel-moisture content in Rothermel's model. The rate of spread for Anderson (1982) fuel model 3 with zero wind and slope is shown.

inducing very strong surface winds, which, in turn, affect the fire. The fire-induced updrafts may also generate pyrocumulus and fire storms. Therefore, a large fire may significantly affect the local atmospheric conditions, creating “its own weather.” The fire-induced convection may lead to formation of a pyro-cumulus cloud and conflagration strong enough to generate its own wind system (a firestorm). See Fromm et al. (2006) and Rosenfeld et al. (2007) for an example of a pyro-convective system generating tornadic winds.

The atmosphere also interacts with the fuel-moisture properties. Periods of warm and hot weather decrease fuel moisture, increasing the fire hazard, and making fires more intense. Conversely, local precipitations or nocturnal moisture recovery tend to decease fuel combustibility and inhibit fire spread. Coupling a weather model with a fire-spread model and a time-lag fuel-moisture model captures these interactions, without explicitly resolving the small-scale combustion and water adsorption processes, in a computationally inexpensive way.

WRF–SFIRE (Mandel et al., 2009, 2011) combines the Weather Research and Forecasting model (WRF) (Skamarock et al., 2008), with the fire-spread model (SFIRE) implemented by the level-set method (Osher and Fedkiw, 2003). WRF–SFIRE is a two-way coupled fire–atmosphere model, so the heat fluxes from the fire component provide forcing to the atmosphere, which influences winds, which in turn modify the fire spread. Similar models include MesoNH-ForeFire (Filippi et al., 2011). Recently, the model was coupled with a fuel-moisture model, and chemical transport of emissions (Fig. 2). The model is able to run faster than real time on several hundred cores, with the fire-model resolution of a few meters and horizontal atmospheric resolution on the order of 100 m for a large real fire (Jordanov

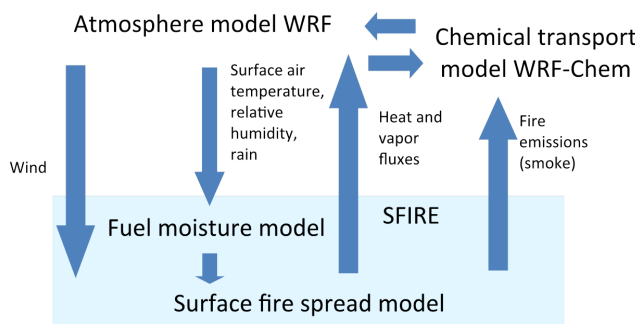


Figure 2. The overall scheme of WRF–SFIRE.

et al., 2012). It can also be run operationally on as little as 24 cores, capturing the basics of wildfire spread on a grid of 40 m, nested within a 400 m cloud-resolving grid.

WRF–SFIRE has evolved from the Coupled Atmosphere–Wildland Fire Environment (CAWFE) (Clark et al., 1996a, b, 2004; Coen, 2005), which consists of the Clark–Hall atmospheric model, coupled with fire spread implemented by tracers. The SFIRE code currently supports the semi-empirical fire-spread model of Rothermel (1972), inherited from the CAWFE code. Implementation of alternative fire-spread models – e.g., Balbi et al. (2009); Fendell and Wolff (2001) – is in progress. The current code and documentation are available from OpenWFM.org. A version from 2010 is distributed with the WRF release as WRF–Fire (Coen et al., 2013; OpenWFM, 2012).

Validation studies of WRF–SFIRE are now available for a large-scale wildfire (Kochanski et al., 2013b), as well as for a microscale simulation of a grass-burn experiment (Kochanski et al., 2013c), fuel-moisture data assimilation (Vejmelka et al., 2014a), and coupling with WRF–Chem (Kochanski et al., 2014b). The coupling of the fire-heat release with the atmosphere enables a detailed study of the effect of wind shear on fire propagation (Kochanski et al., 2013a). Examples of work from other groups using WRF–SFIRE include Simpson et al. (2013) and Peace et al. (2011).

For the first time, this paper describes new developments in the SFIRE software system during the 2 years since the last reference paper by Mandel et al. (2011), and new results demonstrate the relevance of each. Potential fire-severity-assessment tools are described in Sect. 2, ignition in the coupled atmosphere–fire model from a developed fire perimeter in Sect. 3, fuel-moisture model in Sect. 4, and assimilation of RAWS fuel-moisture data in Sect. 5. New software developments include direct input of data in GeoTIFF format (Sect. 6), coupling with smoke transport and atmospheric chemistry by WRF–Chem (Sect. 7), and an operational deployment (Sect. 8). We do not describe the basic principles, operation, or history of the core of WRF–SFIRE here, and refer to Mandel et al. (2011) and the User’s Guide (OpenWFM, 2013) instead.

2 Mapping the severity of a potential fire

WRF–SFIRE users wanted to know “how bad would a fire be” for any particular location, and “how hard would it be to suppress?” Such assessments help the authorities with declaring fire bans and with the allocation of firefighting and fire-prevention resources. Therefore, variables characterizing a potential fire are of interest and they can be used to plot potential fire severity maps. This is a concept similar to FLAMMAP, which computes various potential fire characteristics (Finney, 2006). A more comprehensive approach to fire risk would need to also involve the probability of fire in any given location, similar to in, e.g., the Wildland Fire Decision Support System (WFDSS, <http://wfdss.usgs.gov>), or Carmel et al. (2009).

One quantity requested was the rate of spread, which is already produced by SFIRE, but only at the fire line, because the fire-spread rate depends on the direction of fire propagation. Therefore, a diagnostic variable was added, equal to the maximal rate of spread in any direction for the modeled wind speed and the land-elevation slope. The maximal rate of spread in any direction is also used to compute the reaction intensity, i.e., the released heat-flux intensity immediately upon ignition, and the fire-line intensity (Byram, 1959), at all grid nodes of the fire model, thus providing a spatial representation of the potential-fire characteristics.

3 Initialization from a fire perimeter

A typical fire model starts a fire simulation from a known ignition point at a known ignition time. However, users are also interested in starting WRF–SFIRE from an existing fire, whose presence has just been detected and mapped. Under these circumstances, the ignition point and ignition time typically become known too late to be relevant for real-time simulation and forecasting. Thus, we are interested in starting a fire simulation from a given fire perimeter at a given time (hereafter referred to as the “perimeter time”). However, the fuel balance and the state of the atmosphere depend on the history of the fire, which is not known.

Our solution is to create an approximate artificial history of the fire based on the given fire perimeter and the perimeter time, the fuel map, and the state of the atmosphere during the period before the perimeter time. The history is encoded as the fire arrival time at the nodes of the fire-model mesh. We then use the artificial-fire arrival time instead of the fire-spread model to burn the fuel and generate the heat release to the atmosphere. Replaying the artificial-fire history enables gradual fuel burn, instead of igniting the whole inside of the fire perimeter at once, and thus allows the fire-induced atmospheric circulation to develop. At the perimeter time, the complete coupled atmosphere–fire model takes over.

In Kondratenko et al. (2011), the fire arrival times inside a given perimeter were approximated based on the distance

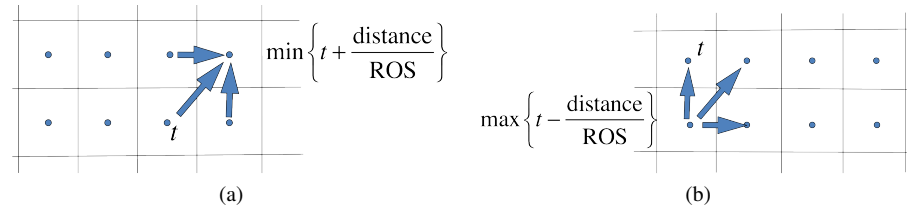


Figure 3. (a) Propagation of ignition time t to a node from neighboring nodes already on fire. (b) Backtracking (propagation back in time) of ignition time to anode from neighboring nodes where the fire arrived later.

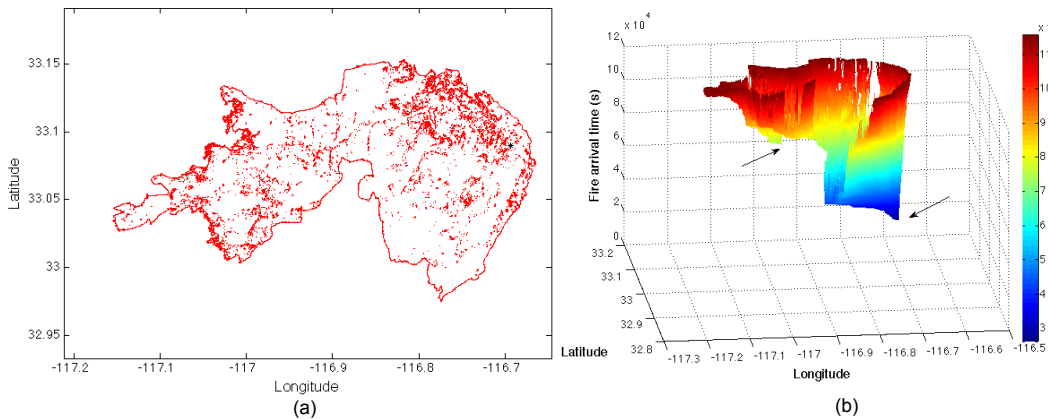


Figure 4. (a) Perimeter of the 2007 Santa Ana fires simulation 22 October 2007, 13:00 PDT (Kochanski et al., 2013b). (b) Artificial-fire arrival time found by fire propagation back in time from the fire perimeter in (a). The fire consisted of two fires, Witch and Guejito, which started on 21 October 2007, 12:15 PDT and 22 October 2007, 13:00 PDT, respectively, and subsequently merged. The two peaks on the bottom, marked by arrows, are the two ignition locations and times, found automatically from the perimeter. The vertical axis and the false color are the time from the beginning of the simulation.

from a known ignition point to the perimeter, while use of the re-initialization equation was proposed in Mandel et al. (2012). Our current approach consists of reversing the direction of time in a fire-spread method, thus shrinking the fire to one or more ignition points. For this purpose, we have developed a new fire-spread method, which is suitable for time reversal. The method determines the ignition time at a node as the earliest time the fire can get to that node from the nodes that are already burning (Fig. 3a). Such methods are known as minimal travel or minimal fire arrival time (Finney, 2002). A list of nodes on the boundary of the already burning region is maintained similarly as in the fast-marching method (Sethian, 1999). However, the fast-marching method cannot be used, because the fire travel time from one node to the next changes dynamically, since it depends on the current wind speed driving the rate of spread in the simulation. To build the artificial fire history, we reverse the direction of the time, replace the minimum in the method by maximum (Fig. 3b), and proceed from the perimeter to the inside of the domain.

Simulation results have shown that the fire can continue in a natural way from the perimeter ignition, for an ideal example (Kondratenko et al., 2011). In this paper, we illustrate perimeter ignition on the simulation of the 2007 Santa Ana fires from Kochanski et al. (2013b). These were two fires,

the Witch fire, and then later the Guejito fire, which merged quickly into one massive fire. The perimeter from the simulation on 22 October 2007, 13:00 PDT, is in Fig. 4a, and the artificial-fire arrival time created is shown in Fig. 4b. The artificial-fire arrival time graph has two minima, which correspond to the two ignition points and times. For the Witch fire, the error in the ignition point location was 3.28 km, which is 5.7 % of the diameter of the given fire perimeter, and the ignition time was exactly the same. For the Guejito fire, the error in the location of the ignition point was 0.04 km, which is 0.07 % of the diameter of the perimeter, and the error in the ignition time was 0.26 h, which is 2.4 % of the time from the ignition to the perimeter time. The root mean square error (RMSE) of the artificial-fire arrival time up to the perimeter time compared to the original simulation was 1199 s. Scaling by the time 24 h 15 m = 81 100 s from the first ignition, 21 October 2007, 12:15 PDT, to the fire perimeter time 22 October 2007, 13:00 PM, gives the relative RMSE of the artificial-fire arrival time only 1.5 %. Figure 5 shows a comparison of the wind from the original simulation and from the spin-up using the artificial-fire arrival time. We have then continued the simulation for additional 8 h to assess the effect of the perimeter ignition on further propagation of the fire (Fig. 6). Again, the original simulation,

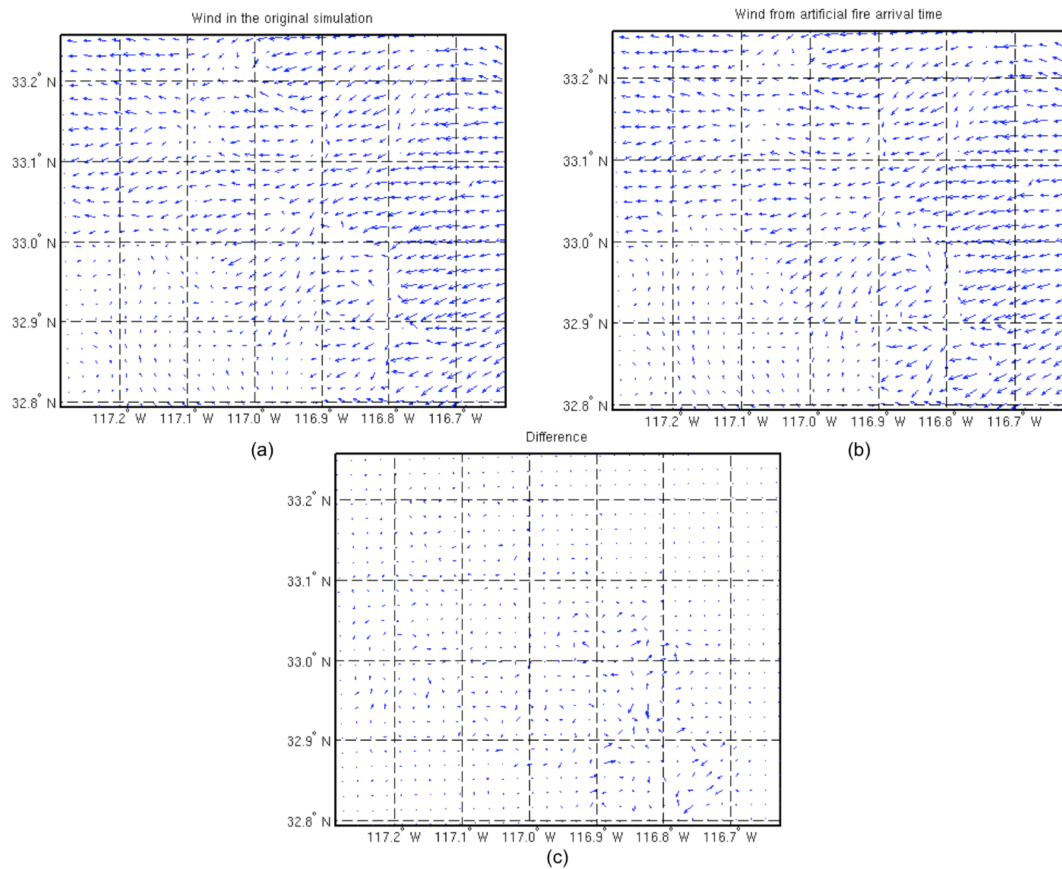


Figure 5. (a) Horizontal wind at 6.1 m in the 2007 Santa Ana fires simulation on October 2007, 13:00 PDT. (b) The same wind as in (a), but with the artificial ignition time history from Fig. 4b until October 2007, 13:00 PDT. The simulation with an artificial fire history, i.e., spin-up, does not use any fire-behavior data from an earlier time, yet the wind fields in each developed quite closely. (c) The difference of (a) and (b). The root mean square error (RMSE) is 1.1 ms^{-1} , which is 8.8 % of the maximal wind speed 12.53 ms^{-1} .

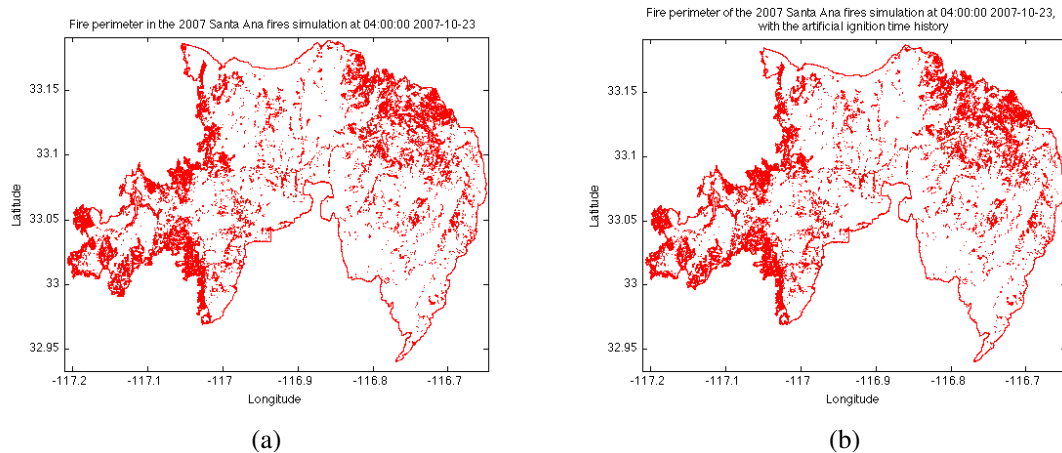


Figure 6. (a) Fire perimeter in the 2007 Santa Ana fires simulation on 22 October 22, 2007, 21:00 PDT. (b) The same perimeter as in (a), but with the artificial-ignition time history from simulation data (Fig. 4b) on 22 October 2007, 13:00 PDT. The simulation with artificial fire history, i.e., spin-up, does not use any fire-behavior data prior to that, yet the differences in the simulation 8 h later are only minor – compare, e.g., the protuberance at the northeast part of the perimeter.

and the simulation started from the perimeter ignition, are quite close, demonstrating the utility of the present approach to simulating the progression of already developed fires detected as perimeters, rather than ignition points. The RMSE of the fire arrival time after continuing from the artificial-fire arrival time for 8 h was 706 s; that is, 2.5 %. This is the error of the perimeter ignition, which was entirely caused by the slight change in the wind at the perimeter time due to the use of the artificial-fire arrival time inside the given perimeter.

4 Fuel-moisture model

Wildfire fuel responds to atmospheric conditions through the evaporation or absorption of moisture from the air, as well as absorbing moisture when it rains. The following simple approach (Kochanski et al., 2012; Mandel et al., 2012) models the evolution of fuel-moisture response by a first-order differential equation, running at each node of the surface mesh independently.

The basic form of the time-lag equation for the moisture content m approaching an equilibrium E with a time lag t_L is

$$\frac{dm}{dt} = \frac{E - m}{t_L}. \quad (1)$$

In the case in which the coefficients E and t_L are constant in time t , the solution of Eq. (1) is

$$m(t) = E + (m(0) - E)e^{-t/t_L}. \quad (2)$$

Thus, the difference of the moisture content m and the equilibrium E decreases to $1 - e^{-1} \approx 0.63$ of its initial value over the time t_L . This is the same definition as used in FARSITE online help (FireModels.org, 2008), and is compatible with the time lag, as used by, e.g., the Wildland Fire Assessment System (WFAS), which is “loosely defined as the time it takes a fuel particle to reach two-thirds of its way to equilibrium with its local environment” (USDA Forest Service, 2014).

Essentially, the simple time-lag model (Eq. 2) considers a fuel particle as a single reservoir with the rate of exchange of water with the environment proportional to the difference from the equilibrium. It is less sophisticated, but much cheaper to run and more data assimilation friendly than the Nelson Jr. (2000) model, now used in the National Fire Danger Rating System (NFDRS), which simulates the dynamics of the water transport in a round wooden stick and the water exchange through the stick surface.

Following the approach from Van Wagner and Pickett (1985, Eqs. 4 and 5), over a long time in constant temperature T (K) and relative humidity H (%), the water content m in dead wood will approach the drying equilibrium:

$$E_d = 0.924H^{0.679} + 0.000499e^{0.1H} + 0.18(21.1 + 273.15 - T)\left(1 - e^{-0.115H}\right),$$

when starting from $m > E_d$, and the wetting equilibrium:

$$E_w = 0.618H^{0.753} + 0.000454e^{0.1H} + 0.18(21.1 + 273.15 - T)\left(1 - e^{-0.115H}\right),$$

when starting from $m < E_w$. The evolution of the fuel moisture in time is thus modeled by the time-lag differential equation with characteristic lag time t_L :

$$\frac{dm}{dt} = \begin{cases} \frac{E_d - m}{t_L} & \text{if } m > E_d \\ 0 & \text{if } E_d \geq m \geq E_w \\ \frac{E_w - m}{t_L} & \text{if } m < E_w \end{cases}. \quad (3)$$

The model is run for $t_L = 1$, 10, and 100 h time-lag fuels, given by the fuel diameter (USDA Forest Service, 2014). Currently, the fuel-moisture equilibrium values for wood are applied to all fuel-moisture classes. The model does not apply to live fuel, which has its own dynamics, on a much longer timescale than a fire-behavior simulation. Therefore, a live fuel-moisture map is entered as a separate fuel class with a very large time lag, and it does not change during the simulation.

During rain, the equilibrium moisture E is taken to be the saturation moisture contents S , and the time lag t_L depends on the rain intensity. A rain-wetting lag time t_r is reached for heavy rain only asymptotically, when the rain intensity r (mm h^{-1}) is large:

$$\frac{dm}{dt} = \frac{S - m}{t_r} \left(1 - \exp\left(-\frac{r - r_0}{r_s}\right)\right), \quad \text{if } r > r_0, \quad (4)$$

where r_0 is the threshold rain intensity, below which no perceptible wetting occurs, and r_s is the saturation rain intensity. At the saturation rain intensity, $1 - 1/e \approx 0.63$ of the maximal rain-wetting rate is achieved. We have calibrated the coefficients to achieve similar behavior to the rain-wetting model in the Canadian fire-danger rating system (Van Wagner and Pickett, 1985), which estimates the fuel moisture as a function of the initial moisture contents and rain accumulation over 24 h. For 10 h fuel, we have obtained the coefficients $S = 250\%$, $t_r = 14\text{ h}$, $r_0 = 0.05\text{ mm h}^{-1}$ and $r_s = 8\text{ mm h}^{-1}$, cf. Fig. 7. This is the default used in the code. Coefficients for specific regions will be, in general, different, and they can be specified by the user as a part of the coded fuel description in WRF–SFIRE. See Vejmelka et al. (2014a) for coefficients obtained by fitting 2 years of data from measurements in Colorado, and a discussion of the modeling errors.

The model maintains the fuel-moisture contents m_k at the center of each atmospheric grid cell on the surface for several fuel classes k , such as 1, 10, 100, and 1000 h fuel. The actual fuel is a mixture of the fuel classes, with w_k denoting the proportion of fuel of class k in the total fuel load, so that the fuel moisture of fine fuels like grass is purely driven by the 1 h fuel moisture, while the fuel moisture of coarser woody fuels is also affected by slower responding 10 and 100 h fuel moisture. The last fuel class is live fuel, whose moisture content is

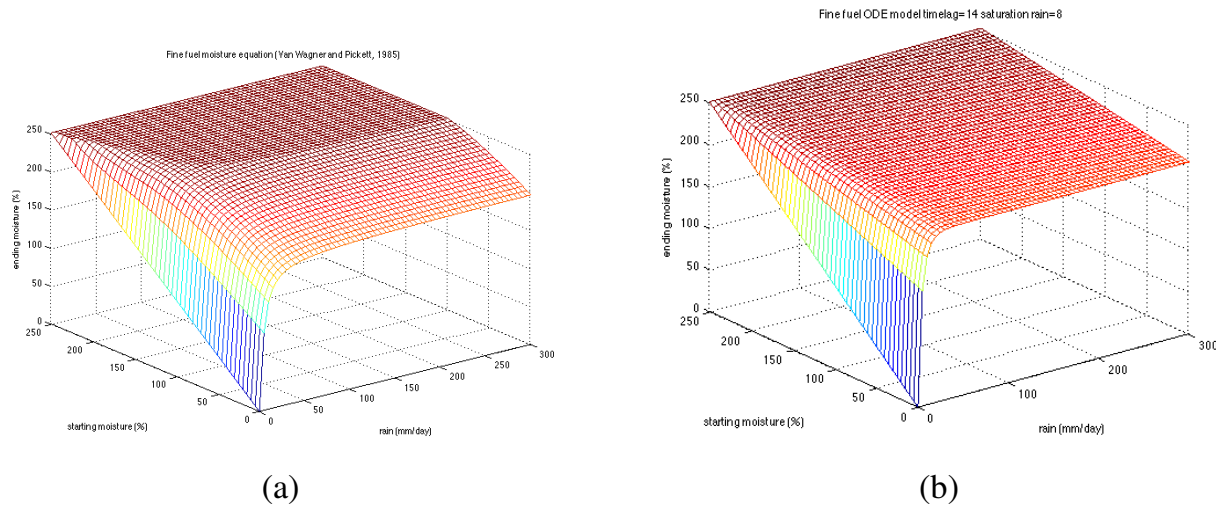


Figure 7. Response of fine fuels to rain over 24 h (a) following Van Wagner and Pickett (1985) (b) from the time-lag model (Eq. 4) by a calibration of coefficients.

given as input data, and it does not change during the simulation. Because the atmospheric mesh is relatively coarse, running the moisture model is not computationally intensive. We also avoid any difficulties with non-homogeneous fuel distribution, because the model is independent of the fuel map. Instead, the proportions $w_k \geq 0$ are obtained from the fuel-category description, e.g., Albini (1976, Table 7, p. 98) or Anderson (1982), with the scaling, so that $\sum_{k=1}^N w_k = 1$. The fuel-moisture contents in each cell on the (finer) fire mesh are then obtained by interpolating the moisture content m_k to the finer grid for each fuel class k , and then computing the weighted average $\sum_{k=1}^N w_k m_k$ with the proportions given by the category of fuel in that cell.

Because the model needs to support an arbitrarily long time step, we have chosen an adaptive exponential method to integrate the fuel-moisture equations at every grid node. On the time interval $[t_n, t_{n+1}]$, we first approximate the equilibria E_d and E_w by constants, derived by averaging the atmospheric state variables at t_n and t_{n+1} , i.e., from $T_{n+1/2} = (T(t_n) + T(t_{n+1}))/2$ for the temperature T , and similarly for the relative humidity H . The rain intensity is determined from the difference in the accumulated rain at the times t_n and t_{n+1} . The solution (Eq. 2) of the resulting constant coefficient equation over the interval $[t_n, t_{n+1}]$ becomes

$$m(t) = m(t_n) + (E_{n+1/2} - m(t_n)) \left(1 - e^{-(t-t_n)/t_L}\right), \quad (5)$$

where $E_{n+1/2}$ is the appropriate equilibrium, E_d , E_w , or S , depending on the value of $m(t_n)$ and if it rains. The time step is performed by evaluating (Eq. 5) at $t = t_{n+1}$, giving

$$m(t_{n+1}) = m(t_n) + (E_{n+1/2} - m(t_n)) \left(1 - e^{-\Delta t/t_L}\right), \quad (6)$$

$$\Delta t = t_{n+1} - t_n.$$

For short time steps, $\Delta t/t_L < \varepsilon = 0.01$, the exponential in Eq. (6) is replaced by the Taylor expansion $1 - e^{-x} \approx x$ to avoid a large relative rounding error caused by subtracting two almost equal quantities. The resulting method is exact for arbitrarily large Δt , when the coefficients are constant in time, and it is of second-order accuracy for smoothly varying coefficients, as $\Delta t \rightarrow 0$.

The fuel-moisture model has been tested during the simulation of the Barker Canyon Complex fire, which started on 8 September 2012, around 20:00 PDT, 10 miles NW from the Grand Coulee Dam in Washington. The 108 h long simulations were performed using a set of five nested domains of gradually increasing resolutions: 36 km, 12 km, 4 km, 1.33 km, and 444 m, with time steps 162, 54, 18, 6, and 2 s, respectively (Fig. 8a). The Mellor–Yamada–Janjic PBL scheme (Janjić, 2001) and the Kain–Fritsch cumulus scheme (Kain and Fritsch, 1990) were used on the three coarsest domains. In order to fully utilize LANDFIRE fuel data and elevation data provided at 30 m resolution, the innermost fire domain had a further-refined fire mesh of 22.2 m (1 : 20 refinement ratio). The atmospheric component of the model was initialized and forced at the boundaries by the North American Regional Reanalysis (NARR), providing meteorological data at 3 h intervals.

There were no ground-fuel-moisture observations available within the fire domain, so the 1 h fuel moisture was initialized with its equilibrium value, while the initial 10, 100, and 1000 h fuel moistures were approximated using data from the National Fuel-Moisture Database (4.0, 8.0, 7.0 %, respectively). The southern branch of the fire was started from the ignition point reported by the Incident Information System (<http://inciweb.nwcg.gov>). The northern branch was ignited using locations of four lightning strikes observed

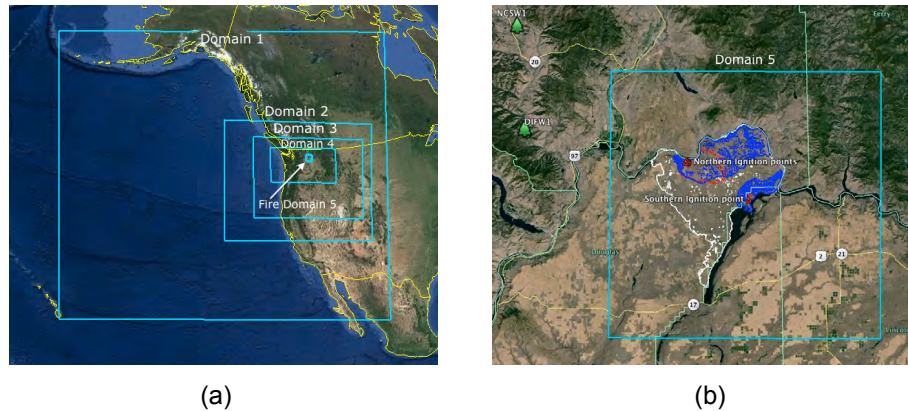


Figure 8. (a) WRF–SFIRE multidomain setup used for the simulation of the 2012 Barker Complex fire (WA). (b) Comparison between the fire perimeters simulated with the constant fuel moisture of 11.6 % (red contour), 6.38 % (white contour), and with the variable fuel moisture simulated by the fuel-moisture model (blue contour). The remotely sensed fire perimeter detected on 13 September 2012 00:44 LT is shown as the green contour. The green tree icons show locations of the Douglas Ingram Ridge (DIFW1) and Cascade Smoke Jumper (NCSW1) stations, reporting 10 h fuel moisture.

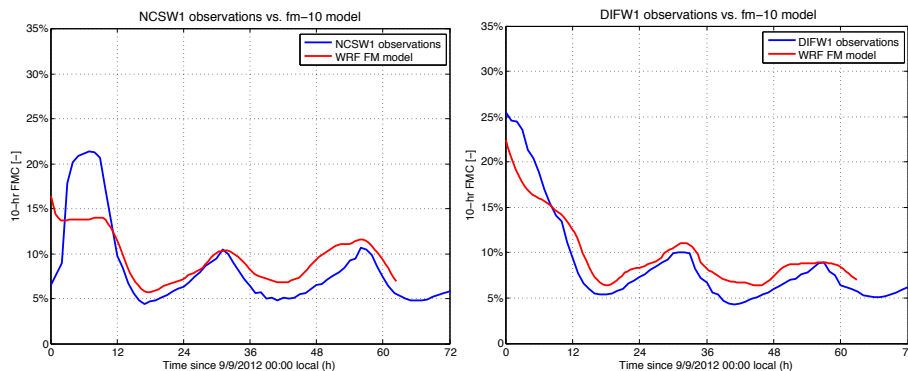


Figure 9. Comparison between the 10 h fuel-moisture observations from the Cascade Smoke Jumper (NCSW1), and the Douglas Ingram Ridge (DIFW1) stations, and simulations from WRF domain 4 with the optimized fuel-moisture parameters set to $S = 2$, $r_k = 1 \text{ mm h}^{-1}$, $r_0 = 0.05 \text{ mm h}^{-1}$, $T_r = 5 \text{ h}$, and the equilibrium E adjusted by $\Delta E = -0.055$.

within the fire perimeter on the ignition day. The approximate locations of the fire-ignition points are presented in Fig. 8b.

For the purpose of a basic validation, the fuel-moisture model has been calibrated and tested against data from the Cascade Smoke Jumper and Douglas Ingram Ridge stations located west of the fire domain (Fig. 8b). Despite the initial biases due to the errors in the WRF-forecasted precipitation at the beginning of the simulation, later into the simulation, the WRF-SFIRE-simulated 10 h fuel moisture closely follows the observed diurnal fuel-moisture fluctuations (Fig. 9). Note that the time series presented in Fig. 9 shows results computed based on 1.33 km resolution meteorological variables from domain 4 after adjustment of fuel-moisture parameters, while the fuel moisture used for the fire-spread simulation (Fig. 10) was computed based on the 444 m resolution meteorological fields from domain 5 data with default fuel-moisture parameters.

In order to assess the impact of the fuel-moisture model on the modeled fire spread, we performed three fire simulations. The first one used the fuel-moisture model, and computed the fuel-moisture changes in all fuel classes based on the local meteorological conditions simulated by the atmospheric component of the system. The other two simulations were performed with temporally and spatially constant fuel moisture. In the first of the other two simulations, the fuel moisture was set to the 4-day average of fuel moisture, simulated using the fuel-moisture model (11.6 %). In the second, the fuel moisture was set to the initial value at the very beginning of the simulation (6.38 %). The time series of the fire area, simulated with the fuel-moisture model and without it using the averaged constant fuel moisture, are presented in Fig. 10. The fire spread clearly responds to the changes in the fuel moisture. The nighttime peaks in the fuel moisture are associated with simulated fire stagnation, while the daytime fuel drying promotes comparatively rapid fire spread. The

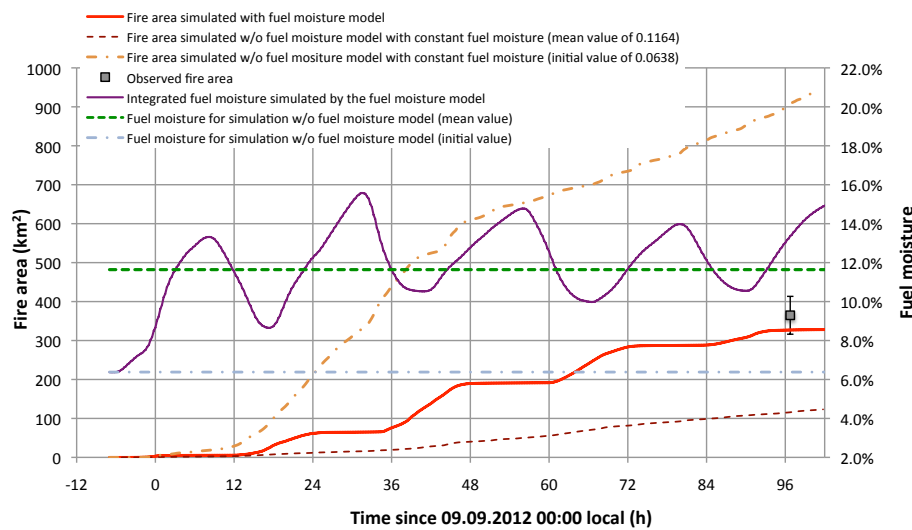


Figure 10. Time series of the WRF–SFIRE simulated fire area (solid lines), and the fuel moisture (dashed lines). The grey point shows the fire area observed on 13 September 2012, 00:44 LT. The error bar shown is estimated from the spread of different reported perimeters. The sunrise in the simulation domain was about 06:30 LT, and the sunset about 19:20 LT. Note that the total fuel moisture contains contributions from all fuel classes as well, not only the fine fuels moisture, resulting in a larger time lag of the total fuel moisture after dawn and dusk.

simulation with the fuel-moisture model not only simulates the diurnal variations in the fire activity, but also improves the total simulated fire area. It is hard to expect the actual fire to exhibit perfectly identical activity patterns each day, and the simulated active fire-spread periods actually varied across the simulation. During all 4 days, the fire exhibited marginal activity during nighttime hours from midnight to 06:00 LT. However, the fire became active between 10:00 LT (day 2) and 13:00 LT (day 3), and ended its progression as early as 08:30 LT (day 4) and as late as midnight (day 3). The sunset at the center of the domain was around 19:22 LT, so the simulated fire remained active between 1 and 4.5 h after sunset. Also, note that Fig. 9 only shows the 10 h fuel-moisture component for the locations of the observational stations, while Fig. 10 shows the total integrated fuel moisture, which is a composite of the 1, 10, 100 h, and live fuel moisture, averaged across the whole fire domain.

The simulation with the constant fuel moisture set to 11.6 % underestimated, in contrast, the fire area by a factor of 3. On the other hand, the simulation performed with the constant fuel moisture initialized with a value corresponding to the initial value in the run with moisture model (6.38 %), overestimated the fire area by a factor of 2. Thus, the run with the fuel-moisture model was a large improvement compared to the simulations with constant fuel moisture, and also successfully captured diurnal variations in the fire activity not present in the run with forecast fuel moisture.

A comparison between the spatial patterns of the Barker Canyon Complex fire simulated with and without the fuel model, as well as the fire perimeter detected on 13 September 2012, 00:44 PDT (108 h after ignition), are presented in Fig. 8b. The fire extent simulated using the constant fuel

moistures (white and red contours) do not compare well with the observations (green contour). The implementation of the time- and spatially-varying fuel moisture significantly improved the simulated fire perimeters of both the northern and the southern branches of the Barker Canyon Complex fire (see the blue contours in Fig. 8b).

5 Assimilation of RAWS fuel-moisture data

To improve the quality of fuel-moisture simulation, we have developed an approach to assimilate fuel-moisture measurements from station measurements. The Remote Automatic Weather Stations (RAWS) in the US also include measurements of fuel moisture. They measure the in situ weight of a sample of 10 h fuel, and the resulting fuel-moisture data are exported to <http://mesowest.utah.edu> continuously. The RAWS data are available hourly, but only at a small number of locations, which generally do not coincide with grid nodes of our simulation grids. Hence, the regression technique, described later in this section, needs to interpolate the covariates from the simulation grid to the RAWS locations.

Even though only 10 h fuel moisture is measured, fuel moisture is simulated independently in three classes: 1, 10, and 100 h. The results are combined for each fuel type according to relative mass contributions derived from Albini (1976). Each fuel class responds to the atmospheric conditions at a different time scale. The data assimilation modifies the equilibria in all fuel classes by a common additive correction. Consequently, changes made by the data assimilation to the 10 h fuel-moisture equilibrium are transferred to 1 and 100 h fuel equilibria as well, even though approaching the

equilibria is still determined by the respective 1 and 100 h time lags.

We follow Vejmelka et al. (2014b, a) with some simplifications. To assimilate the moisture measurement into the model (Eq. 3) with N_k dead fuel classes at each grid point, we augment the model state $(m_k)_{k=1,\dots,N_k}$ by perturbations ΔE and ΔS of the equilibrium moisture values: we replace E_d , E_w , and S in Eq. (3), by $E_d + \Delta E$, $E_w + \Delta E$, and $S + \Delta S$, respectively, and add the differential equations $d\Delta E/dt = 0$, $d\Delta S/dt = 0$. We then apply the standard extended Kalman filter to the model in the augmented variables:

$$\mathbf{m}(t_i) = (m_1(t_i), m_2(t_i), \dots, m_{N_k}(t_i), \Delta E(t_i), \Delta S(t_i)).$$

Note that the common state variables ΔE and ΔS now couple the evolution of the different time-lag fuel-moisture classes together.

We extend the measurements and their uncertainty from several RAWS locations to the whole domain using a trend surface model (Schabenberger and Gotway, 2005, Sect. 5.3.1). We look for a fuel-moisture estimate $Z(s)$ at a location s in the form

$$Z(s) = X_1(s)\beta_1 + \dots + X_k(s)\beta_k + e(s), \quad (7)$$

where the fields X_j are given fields, called covariates, and the errors $e(s) \sim N(0, \hat{\sigma}^2)$ are independent, with $\hat{\sigma}^2$ the variance of the so-called microscale variability (i.e., the part of the structure of the spatial random field that is too small to be captured by the mesh). Given the measurements $\hat{Z}(s_i)$, $i = 1, \dots, n$, the coefficients β_j are found from the regression:

$$\begin{aligned} \hat{Z}(s_i) &= X_1(s_i)\beta_1 + \dots + X_k(s_i)\beta_k + \varepsilon(s_i) + e(s_i), \\ i &= 1, \dots, n, \end{aligned} \quad (8)$$

where the errors $\varepsilon(s_i) \sim N(0, \gamma^2)$ are assumed to be independent, and also independent of $e(s_j)$. The variance γ^2 models the measurement error at the measurement-station locations s_1, \dots, s_n . See Vejmelka et al. (2014b) for a generalization on when γ^2 is allowed to be different at different locations s_i .

The solution of the regression problem (Eq. 8) is obtained as the least-squares solution:

$$\beta = (X(s)^T X(s))^{-1} X(s)^T \hat{Z}(s), \quad (9)$$

where

$$\begin{aligned} \beta &= \begin{bmatrix} \beta_1 \\ \vdots \\ \beta_k \end{bmatrix}, X(s) = \begin{bmatrix} X_1(s_1) & \dots & X_k(s_1) \\ \vdots & \ddots & \vdots \\ X_1(s_n) & \dots & X_k(s_n) \end{bmatrix}, \\ \hat{Z}(s) &= \begin{bmatrix} \hat{Z}(s_1) \\ \vdots \\ \hat{Z}(s_k) \end{bmatrix}. \end{aligned} \quad (10)$$

We then have the well-known unbiased estimate of the residual variance from the residual sum of squares:

$$\begin{aligned} \gamma^2 + \hat{\sigma}^2 &= \frac{1}{n-k} \sum_{i=1}^n \hat{e}(s_i)^2, \hat{e}(s_i) = \hat{Z}(s_i) \\ &\quad - (X_1(s_i)\beta_1 + \dots + X_k(s_i)\beta_k). \end{aligned} \quad (11)$$

The mean and the variance of the estimated field $Z(s)$ are obtained by computing the least-squares solution β from Eq. (8) and substituting into the trend surface model (Eq. 7), which gives

$$\mathbf{EZ}(s) = X_1(s)\beta_1 + \dots + X_k(s)\beta_k$$

with the mean-squared prediction error

$$\text{Var } Z(s) = \hat{\sigma}^2 + (\gamma^2 + \hat{\sigma}^2) \mathbf{x}(s)^T (X(s)^T X(s))^{-1} \mathbf{x}(s),$$

where $\mathbf{x}(s) = t[X_1(s), \dots, X_k(s)]^T$.

We use $k = 8$ covariates. The first four covariates are taken to be the current forecast of 10 h fuel moisture, air temperature at 2 m, the surface pressure, and the current rain intensity, which capture the effect of the local state of the atmosphere on the fuel-moisture equilibrium. The remaining covariates are the terrain elevations, and three independent functions linear in space, taken as the longitude, the latitude, and a constant. These covariates were found to result in the best prediction from several alternatives. With these covariates, the trend surface model alone gave better results than the inverse square distance interpolation method used in the WFAS (Burgan et al., 1998), and employing the extended Kalman filter resulted in a further improvement (Vejmelka et al., 2014a, Fig. 3).

6 Data management and visualization

WRF–SFIRE input uses, in part, the standard WRF inputs, prepared by the WRF Preprocessing System (WPS) in WRF. In addition to meteorological data needed for WRF, SFIRE also requires high-resolution topography and fuel maps. These are, however, typically available in GeoTIFF format, rather than one of the formats employed by WPS, which was created primarily for processing atmospheric data.

GeoTIFF is a standard for georeferencing metadata in Tagged Image File Format (TIFF) files (Ritter and Ruth, 2000). The GeoTIFF format is particularly useful for fire-related data and fine-scale topography, because it enables a compact representation of data on large meshes with thousand of cells (pixels) in each dimension.

GeoTIFF support has been added to WRF–SFIRE in two forms (Beezley et al., 2011). First, GeoTIFF can be converted into Geogrid files, which can be read by any standard installation of WPS by a separate utility. This utility, which has a command line, flags to control various Geogrid attributes,

such as the size of the tiles. The utility creates a header that contains both a description of the tiles and the geocoding (projection and reference points). TopoGrabber (<http://laps.noaa.gov/topograbber>) is a Python application based on this conversion utility, which is capable of downloading and converting topographical data automatically.

Conversion of GeoTIFF files, however, creates large Geogrid files, which can present difficulties. For this reason, the WPS has been modified to read GeoTIFF files directly. Here, the GeoTIFF library is wrapped around an abstraction layer that reads the data in tiles. The main advantage is that it can read floating point data directly, rather than needing to convert to and from fixed point, as required by the Geogrid file format, and thus it can handle large meshes more easily. Such meshes occur naturally as a consequence of high-resolution fire modeling.

NetCDF is the standard file format for WRF output files. Visualization pathways that utilize WRF–SFIRE output files in the NetCDF format include VAPOR and KML format for Google Maps and Google Earth (Beezley et al., 2012). What has caught the most attention is the utility posted at <https://github.com/jbeezley/wrf2kmz>. This utility processes the NetCDF files from WRF–SFIRE into KML and the compressed variant KMZ, using several Python libraries. This is the software used to generate the Google Maps and Google Earth images in this paper and in our previous work, referenced here. It is also behind the prototype web interface (Beezley et al., 2012), as well as the Israeli national operational system, described in Sect. 8.

7 Coupling with smoke transport and chemistry

Fire emissions from SFIRE can be input into WRF–Chem (Grell et al., 2005) as chemical species, or into the WRF dynamical core as passive tracers. Chemical species are available only when WRF is built with the Chem component, while the smoke representation in passive tracers is available, even in the base WRF code. This has a significant advantage, because the full WRF–Chem execution is very computationally intensive, and setting up the coupled WRF–Chem–SFIRE model is much more difficult. Both kinds of fire emissions are handled by SFIRE in the same way, transparently to the user.

The chemical emissions from a fire are modeled as the mass of the fuel burned times the emission factor for each species, specified in a configuration file as a text table. Files with emission factors from FINN (Wiedinmyer et al., 2011) for the regional acid deposition model (RADM) and model of ozone and related chemical tracers (MOZART) chemical mechanisms, supported by WRF–Chem, are supplied with the code. The table contains one line for each chemical species, with the amount per kilograms of fuel burned for each fuel category. Gas emissions and particulate emissions ($\text{PM}_{2.5}$ and PM_{10}) are given in g kg^{-1} , and non-methane

organic carbon emissions in mol kg^{-1} . In every time step, the mass of every species emitted from the burning fuel during the time step is converted to appropriate concentrations in the first layer of cells in the atmospheric grid in WRF, and added to the concentrations of the chemical species advected by the atmosphere and subject to chemical reactions modeled by WRF–Chem.

WRF, with or without Chem, can be run with eight passive tracers, which are advected by the atmospheric winds without any chemical reactions. One is a basic tracer, simply advected by the wind field, other passive tracers have various special properties (e.g., diffusion). Emission factors for the tracers are specified in the same configuration file as the chemical species, in each fuel category. Just like the chemical species, passive tracer emissions are converted by the coupling code to concentrations in the first layer of the atmospheric grid in WRF, and added to the tracer concentration. Unlike WRF–Chem, which is very computationally intensive, turning on the tracers has only a minimal effect on the computational cost. Therefore, modeling–emission transport by the passive tracers is well suited for forecasting in real time.

See the WRF–SFIRE Users' Guide (OpenWFM, 2013) for more details on use, and Kochanski et al. (2014a, b) for further justification and experimental results. Figure 11 illustrates the simulation of emissions from a large fire.

It is noteworthy that the described coupling also includes integration with aerosol schemes. Depending on the selected options in WRF–Chem, the chemical species emitted from the fire may react in the atmosphere, leading not only to secondary pollutants formations, but also to secondary aerosols. The chemical species emitted and formed in the atmosphere, as well as primary and secondary aerosols, may impact radiative and microphysical processes, thus adding new levels of coupling between the fire and the atmosphere.

In the simplified emissions model used, the emissions are fuel specific and defined per mass of burned fuel. Hence, only the fuel consumption rate (mass/unit time) is used for the computation of the emission fluxes. In future versions, we will consider supporting emission factors dependent on fire characteristics, such as the fire intensity and fuel fraction, and distinguishing empirically between the flaming and smoldering stages of fire.

So far, the simulated $\text{PM}_{2.5}$, NO , O_3 , and plume height have been tested against observations (Kochanski et al., 2014b). The results of coupling with aerosol schemes have not yet been validated.

8 Operational use in Israel

The Israeli national fire forecasting system¹ is built on top of WRF–SFIRE. From the advances described in this paper, the

¹The Israel national fire forecasting system is an initiative of the Israel Public Security ministry.

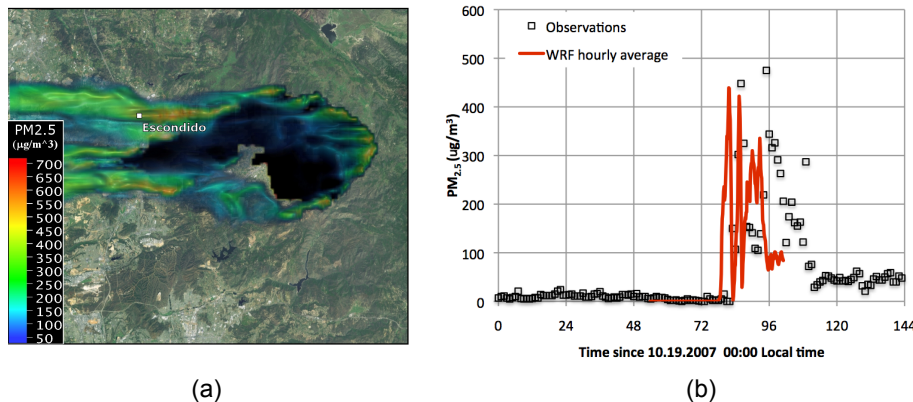


Figure 11. An example of the PM_{2.5} concentration field in $\mu\text{g m}^{-3}$, simulated for the Witch and Guejito fires in California using WRF–SFIRE–Chem. (a) Simulated PM_{2.5} on 22 October 2007, 13:00 LT (hour 85 since 19 October 2007, 00:00 LT) with the location of the Escondido air-quality station. Only concentrations above 50 $\mu\text{g m}^{-3}$ are shown, and the black fill in the background represents the burnt area, (b) Simulated hourly averaged PM_{2.5} (red line) and observations (black points) from Escondido air-quality station, marked as the white squares on (a).



Figure 12. Weather forecast for Israel, which serves as a basis for the fire forecast. Wind and temperature shown to the user.

system uses the potential fire behavior (Sect. 2), the moisture model (Sect. 4), and the geographic information system (GIS) data sources and conversions (Sect. 6). For operational reasons, this deployment uses coarser meshes on a smaller number of processors. The effect of the feedback from the fire to the atmosphere is reduced, but the benefits of the tight (coupled) integration of the fire simulation with a fine-scale weather forecast remain.

The system is based on a complete WRF mesoscale weather forecast for Israel (Fig. 12). In order to be able to produce a fire forecast on demand, the weather forecasting system uses National Weather Service (NWS) data four times daily, refined into hourly WRF forecasts, from

which the fire forecast is made. The WRF forecasts are at a 1.333 km resolution (higher than the NWS forecasts), and then they are dynamically downscaled by nesting a 444 m grid within the 1.333 km mesh, similarly as in Fig. 8. The coupled atmosphere–fire model then runs with 444 m atmospheric mesh resolution and 44.4 m fire mesh resolution. This system can provide not only fires forecast, but also high-resolution forecasts of severe weather winds/hail, precipitation fields, and terrain-sensitive snow amounts.

Once a day, the moisture model is run with a 1.333 km resolution and a 1 h time step from the 24 h weather forecast. The output of the fuel-moisture model is then interpolated to 444 m and provided to the fire model hourly.



Figure 13. Interactive fire ignition.

The fire forecasting system works interactively via a web interface. When a fire is detected, the user pins the location of the fire by clicking on the interactive map (Fig. 13), or enters the location numerically. The web site then notifies the server system that a WRF–SFIRE forecast has been requested. Given the ignition point, a Python script on the server generates a series of name lists with the correct parameters describing the fire simulation domain, which has 36×36 cells on the atmospheric 444 m mesh, and 360×360 cells on the fire 44 m mesh. The ignition point is as close to the center as possible. Static surface data on the fire simulation grid are generated and downscaled data from the 1.333 km simulation, and the fuel-moisture forecast at 444 m are interpolated to the fire mesh grid.

In about 10–12 min, the first hour of the forecast is produced, and within 30 min, a 6 h fire forecast is staged for download on the website. In addition to animations, the web site also creates Google Earth-based maps of fire spread, intensity, and area coverage. A screen snapshot from the forecast of the 2013 Eshtaol fire in Israel is in Fig. 14. The forest fire caused the authorities to block road 38 for 3 h, until they controlled the fire intensity by utilizing ground and aerial suppression.

The fuel maps are an aggregate of three sources. GIS maps of forests from the Jewish National Fund (JNF)'s field operations are overlaid by a GIS land-use map from Israeli national archives. Both are at a 61 m resolution. The third source is the US Geological Survey (USGS) 1 km resolution vegetation map, which pads the missing data around the Israeli border and inside the Palestinian authority. Since Rothermel's rate of spread model was not developed for Mediterranean conditions, the system supports rate of spread correction factors

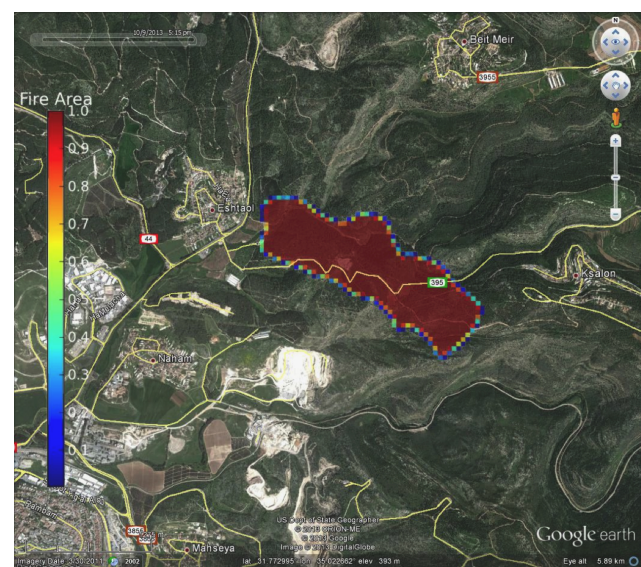


Figure 14. Fire area and fire-line forecast for the fire area of a real fire that was ignited at 11:15 LT, 9 October 2013. Fire area value of 1.0 means that the whole grid cell is burning.

in order to enable applying the modified rates of spread, as suggested by Carmel et al. (2009). Specifically, the rates of spread are reduced by a factor of 2 for Anderson (1982) fuel models 1 and 4, and by a factor of 4 for fuel model 10.

The system also provides an estimate of how bad the fire would be if a specified location were to burn. Measures of the severity of such potential fires are computed along with the fine-resolution weather forecast in every cell of the fire model. The first such measure is the maximum rate of spread



Figure 15. Fire-risk forecast for Israel, computed as the maximal rate of spread in any direction, and rescaled so that the maximum possible fire rate of spread from Rothermel's model corresponds to value of 5.

in any direction, computed from the fuel category in the cell, the forecasts of fuel moisture, and forecast of the wind vector, in exactly the same way as that in the fire simulation. The fire intensity and fire-line intensity are then derived from the maximum rate of spread in any direction (Sect. 2). The code provides these values at all nodes of the fire model grid. However, our users were interested in a simplified interface with the values only shown at several select points. Therefore, only the values of the fire-line intensity, rescaled to the range 0 to 5 at several landmark points, are presented to the web user (Fig. 15), instead of a map with several layers.

Validation of the system currently relies on existing validation studies for WRF–SFIRE (Kochanski et al., 2013b, c). Validation for local conditions, including fuel types, maps, and the effect of the moisture model, is in progress.

The WRF–SFIRE system can provide a valuable and helpful tool to users. Currently, it is the only fire model running in Israel operationally, and, as far as we know, the only coupled fire–atmosphere model running operationally anywhere. In addition, the weather forecasts themselves are not standard NWS products, but rather predict the weather at the scale of the fire attack crews. The system is delivered to subscribers in the firefighting community and other users in Israel to forecast the fire spread and assess the difficulty of suppression and fire danger (Regev et al., 2012).

9 Summary and conclusions

WRF–SFIRE system has significantly evolved since its original description was published in Mandel et al. (2009, 2011). The originally simple fire-modeling framework was

advanced by new components, which significantly expanded the original capabilities of WRF–SFIRE. The coupling between the atmospheric component of the system and the fuel-moisture model enables modeling the fire spread while taking into account dynamic changes in the fuel properties driven by the weather conditions. In the current form, the model not only creates a weather forecast, but also a fuel-moisture forecast, which is used by the fire component of the system to simulate the fire behavior. This new level of interaction embedded into the WRF–SFIRE modeling system has the potential to improve fire-behavior representation when temporal changes in the fuel moisture affect fire spread. The model does not assume any diurnal variation in the fuel moisture or intensity. Instead, basic atmospheric properties, including temperature, humidity, precipitation, and winds, are used for the computation of the fuel moisture and the fire spread at any given time. The fuel-moisture component of the system is also used as the core of a fuel-moisture-data-assimilation system, which creates the best estimate of the fuel-moisture state, generated in a gridded form by a fusion of the observed fuel moisture with the moisture-model estimates.

The updated version also simulates the fire smoke. Depending on the users' requirements, smoke can be simply treated as a passive tracer advected in the dynamical core of the WRF model, or represented as a mixture of chemically reactive species emitted into the atmosphere, and undergoing chemical and physical reactions. The latter approach, requiring building the model with WRF–Chem, not only allows the study fire and smoke emission and dispersion, but also an investigation of the effects of smoke on atmospheric chemistry. The coupling between the fire model and the chemistry

provides a new framework for simulating secondary pollutants created in the atmosphere from the species emitted directly by the fire, which is of interest in estimating the air quality effects of the fire emissions.

The integration with the WRF–Chem is not limited to chemical species. The primary aerosols and creation of secondary aerosols may be captured with this framework as well. The aerosols emitted by fires may interact with radiation and microphysical processes, allowing for another level of coupling between the fire and atmosphere, which is needed, for example, in order to study processes related to creation of pyro-cumulus clouds.

The original point and line ignitions have been expanded by incorporating ignition from a fire perimeter given by the user (e.g., from remote sensing). This new functionality continues the coupled atmosphere–fire simulation from a given fire contour, without the need for starting the simulation from an initial ignition point or line.

In conclusion, advances in the WRF–SFIRE system include coupling, which can have a significant impact on fire behavior (moisture), or are significantly impacted by fire (atmospheric chemistry). Improvements have also been directed towards increasing usability in practice (interfaces with the GIS, potential fire severity assessment, and ignition from a given perimeter). WRF–SFIRE benefits from the integration with WRF, the widespread use of WRF, distribution in the public domain, the general knowledge of operating WRF in the atmospheric science community, and it leverages the standard WRF inputs and outputs.

As a consequence, WRF–SFIRE has become the first two-way coupled fire–atmosphere model implemented operationally. The newly added capabilities, in terms of smoke- and fire-emission prediction, mean that WRF–SFIRE is an “all-in-one model” with a potential of generating fire spread, fire emission, plume rise, plume dispersion, and air quality forecast within one integrated framework.

Future work will expand the perimeter-ignition approach to the assimilation of fire-behavior data, particularly fire locations from remote sensing. Addition of new fire-spread models, as well as mechanisms for integration with other systems, such as Blue Sky and CMAQ, are also planned.

Acknowledgements. This research was partially supported by the National Science Foundation (NSF) grants AGS-0835579 and DMS-1216481, and the National Aeronautics and Space Administration (NASA) grants NNX12AQ85G and NNX13AH9G. This work partially utilized the Janus supercomputer, supported by the NSF grant CNS-0821794, the University of Colorado Boulder, University of Colorado Denver, and National Center for Atmospheric Research. The wildfire system for Israel was funded by the Israel Public Security Ministry.

Edited by: J.-B. Filippi

Reviewed by: two anonymous referees

References

- Albini, F. A.: Estimating wildfire behavior and effects, US Forest Service, General Technical Report INT-30, <http://www.treesearch.fs.fed.us/pubs/29574> (last access: October 2014), 1976.
- Albini, F. A.: A model for the wind-blown flame from a line fire, *Combustion and Flame*, 43, 155–174, doi:10.1016/0010-2180(81)90014-6, 1981.
- Albini, F. A.: Response of Free-Burning Fires to Non-steady Wind, *Combust. Sci. Technol.*, 29, 225–241, doi:10.1080/00102208208923599, 1982.
- Anderson, H. E.: Aids to determining fuel models for estimating fire behavior, USDA Forest Service General Technical Report INT-122, http://www.fs.fed.us/rm/pubs_int/int_gtr122.html (last access: October 2014), 1982.
- Balbi, J. H., Morandini, F., Silvani, X., Filippi, J. B., and Rinieri, F.: A physical model for wildland fires, *Combust. Flame*, 156, 2217–2230, doi:10.1016/j.combustflame.2009.07.010, 2009.
- Beer, T.: The interaction of wind and fire, *Bound.-Lay. Meteorol.*, 54, 287–308, doi:10.1007/BF00183958, 1991.
- Beezley, J. D., Kochanski, A. K., and Mandel, J.: Integrating high-resolution static data into WRF for real fire simulations, Paper 6.3, Ninth Symposium on Fire and Forest Meteorology, Palm Springs, October 2011, <http://ams.confex.com/ams/9FIRE/webprogram/Paper192276.html>, retrieved December 2011.
- Beezley, J. D., Martin, M., Rosen, P., Mandel, J., and Kochanski, A. K.: Data management and analysis with WRF and SFIRE, *IEEE Geosci. Remote Sens.*, 2012, 5274–5277, doi:10.1109/IGARSS.2012.6352419, 2012.
- Burgan, R. E., Klaver, R. W., and Klaver, J. M.: Fuel models and fire potential from satellite and surface observations, *Int. J. Wildland Fire*, 8, 159–170, 1998.
- Byram, G. M.: Combustion of forest fuels, in: *Forest Fire: Control and Use*, edited by: Davis, K. P., McGraw Hill, New York, 61–89, 1959.
- Carmel, Y., Paz, S., Jahashan, F., and Shoshany, M.: Assessing fire risk using Monte Carlo simulations of fire spread, *Forest Ecol. Manage.*, 257, 370–377, doi:10.1016/j.foreco.2008.09.039, 2009.
- Clark, T. L., Jenkins, M. A., Coen, J., and Packham, D.: A Coupled Atmospheric-Fire Model: Convective Feedback on Fire Line Dynamics, *J. Appl. Meteorol.*, 35, 875–901, doi:10.1175/1520-0450(1996)035<0875:ACAMCF>2.0.CO;2, 1996a.
- Clark, T. L., Jenkins, M. A., Coen, J. L., and Packham, D. R.: A coupled atmosphere-fire model: Role of the convective Froude number and dynamic fingering at the fireline, *Int. J. Wildland Fire*, 6, 177–190, doi:10.1071/WF9960177, 1996b.
- Clark, T. L., Coen, J., and Latham, D.: Description of a Coupled Atmosphere-Fire Model, *Int. J. Wildland Fire*, 13, 49–64, doi:10.1071/WF03043, 2004.
- Coen, J. L.: Simulation of the Big Elk Fire using coupled atmosphere-fire modeling, *Int. J. Wildland Fire*, 14, 49–59, doi:10.1071/WF04047, 2005.
- Coen, J. L., Cameron, M., Michalakes, J., Patton, E. G., Riggan, P. J., and Yedinak, K.: WRF-Fire: Coupled Weather-Wildland Fire Modeling with the Weather Research and Forecasting Model, *J. Appl. Meteor. Climatol.*, 52, 16–38, doi:10.1175/JAMC-D-12-023.1, 2013.

- Fendell, F. E. and Wolff, M. F.: Wind-aided fire spread, in: Forest fires, behavior and ecological effects, edited by: Johnson, E. A. and Miyanishi, K., Academic Press, San Diego, CA, 171–223, 2001.
- Filippi, J. B., Bosseur, F., Pialat, X., Santoni, P., Strada, S., and Mari, C.: Simulation of coupled fire/atmosphere interaction with the MesoNH-ForeFire models, *J. Combust.*, 2011, 540390, doi:10.1155/2011/540390, 2011.
- Finney, M. A.: Fire growth using minimum travel time methods, *Can. J. Forest Res.*, 32, 1420–1424, doi:10.1139/x02-068, 2002.
- Finney, M. A.: An overview of FlamMap fire modeling capabilities, in: Fuels Management – How to Measure Success, edited by Andrews, P. L. and Butler, B. W., USDA Forest Service, proceedings RMRS-P-41, available at: <http://www.treesearch.fs.fed.us/pubs/25948>, 213–220, 2006.
- FireModels.org: FARSITE Program Download, Version 4.1.055, <http://www.firemodels.org/index.php/farsite-software/farsite-downloads> (retrieved: July 2014), 2008.
- Fromm, M., Tupper, A., Rosenfeld, D., Servranckx, R., and McRae, R.: Violent pyro-convective storm devastates Australia's capital and pollutes the stratosphere, *Geophys. Res. Lett.*, 33, L05815, doi:10.1029/2005GL025161, 2006.
- Grell, G. A., Peckham, S. E., Schmitz, R., McKeen, S. A., Frost, G., Skamarock, W. C., and Eder, B.: Fully coupled “online” chemistry within the WRF model, *Atmos. Environ.*, 39, 6957–6975, doi:10.1016/j.atmosenv.2005.04.027, 2005.
- Janjić, Z. I.: Nonsingular implementation of the Mellor-Yamada level 2.5 scheme in the NCEP Meso model, NCEP Office Note No. 437, available at <http://www.emc.ncep.noaa.gov/officenotes/newernotes/on437.pdf> (retrieved: May 2014), 2001.
- Jordanov, G., Beezley, J. D., Dobrinkova, N., Kochanski, A. K., Mandel, J., and Sousedík, B.: Simulation of the 2009 Harmanli fire (Bulgaria), in: 8th International Conference on Large-Scale Scientific Computations, Sozopol, Bulgaria, 6–10 June 2011, edited by: Lirkov, I., Margenov, S., and Waniewski, J., vol. 7116 of Lecture Notes in Computer Science, Springer, Berlin, Heidelberg, 291–298, doi:10.1007/978-3-642-29843-1_33, also available as arXiv:1106.4736, 2012.
- Kain, J. S. and Fritsch, J. M.: A One-Dimensional Entrainning/Detraining Plume Model and Its Application in Convective Parameterization, *J. Atmos. Sci.*, 47, 2784–2802, doi:10.1175/1520-0469(1990)047<2784:AODEPM>2.0.CO;2, 1990.
- Kochanski, A. K., Beezley, J. D., Mandel, J., and Kim, M.: WRF fire simulation coupled with a fuel moisture model and smoke transport by WRF-Chem, 13th WRF Users' Workshop, National Center for Atmospheric Research, 20–24 June 2012, arXiv:1208.1059, 2012.
- Kochanski, A. K., Jenkins, M. A., Sun, R., Krueger, S., Abedi, S., and Charney, J.: The importance of low-level environmental vertical wind shear to wildfire propagation: Proof of concept, *J. Geophys. Res.-Atmos.*, 118, 8238–8252, doi:10.1002/jgrd.50436, 2013a.
- Kochanski, A. K., Jenkins, M. A., Krueger, S. K., Mandel, J., and Beezley, J. D.: Real time simulation of 2007 Santa Ana fires, *Forest Ecol. Manage.*, 15, 136–149, doi:10.1016/j.foreco.2012.12.014, 2013b.
- Kochanski, A. K., Jenkins, M. A., Mandel, J., Beezley, J. D., Clements, C. B., and Krueger, S.: Evaluation of WRF-SFIRE performance with field observations from the FireFlux experiment, *Geosci. Model Dev.*, 6, 1109–1126, doi:10.5194/gmd-6-1109-2013, 2013c.
- Kochanski, A. K., Beezley, J. D., Mandel, J., and Clements, C. B.: Air pollution forecasting by coupled atmosphere-fire model WRF and SFIRE with WRF-Chem, in: Proceedings of 4th Fire Behavior and Fuels Conference, 18–22 February 2013, Raleigh, NC and 1–4 July 2013, St. Petersburg, Russia, edited by Wade, D. D. and Fox, R. L., 143–155, International Association of Wildland Fire, Missoula, MT, compiled by: Robinson, M. L., available at: http://www.iawfonline.org/4th_Fuels_Conference_Proceedings_USA-Russia.pdf (last access: July 2014), 2014a.
- Kochanski, A. K., Jenkins, M. A., Yedinak, K., Mandel, J., Beezley, J., and Lamb, B.: Toward an integrated system for fire, smoke, and air quality simulations, arXiv:1405.4058, *Int. J. Wildland Fire*, to appear, 2014b.
- Kondratenko, V. Y., Beezley, J. D., Kochanski, A. K., and Mandel, J.: Ignition from a Fire Perimeter in a WRF Wildland Fire Model, Paper 9.6, 12th WRF Users' Workshop, National Center for Atmospheric Research, 20–24 June 2011, <http://www.mmm.ucar.edu/wrf/users/workshops/WS2011/WorkshopPapers.php>, retrieved: August 2011.
- Linn, R. R. and Cunningham, P.: Numerical simulations of grass fires using a coupled atmosphere-fire model: Basic fire behavior and dependence on wind speed, *J. Geophys. Res.-Atmos.*, 110, D13107, doi:10.1029/2004JD005597, 2005.
- Mandel, J., Beezley, J. D., Coen, J. L., and Kim, M.: Data Assimilation for Wildland Fires: Ensemble Kalman filters in coupled atmosphere-surface models, *IEEE Control Syst. Mag.*, 29, 47–65, doi:10.1109/MCS.2009.932224, 2009.
- Mandel, J., Beezley, J. D., and Kochanski, A. K.: Coupled atmosphere-wildland fire modeling with WRF 3.3 and SFIRE 2011, *Geosci. Model Dev.*, 4, 591–610, doi:10.5194/gmd-4-591-2011, 2011.
- Mandel, J., Beezley, J. D., Kochanski, A. K., Kondratenko, V. Y., and Kim, M.: Assimilation of Perimeter Data and Coupling with Fuel Moisture in a Wildland Fire – Atmosphere DDDAS, *Procedia Comput. Sci.*, 9, 1100–1109, doi:10.1016/j.procs.2012.04.119, 2012.
- Matthews, S., J., G., and McCaw, L.: Simple models for predicting dead fuel moisture in eucalyptus forests, *Int. J. Wildland Fire*, 19, 459–467, doi:10.1071/WF09005, 2010.
- Mell, W., Jenkins, M. A., Gould, J., and Cheney, P.: A physics-based approach to modelling grassland fires, *Intl. J. Wildland Fire*, 16, 1–22, doi:10.1071/WF06002, 2007.
- Nelson Jr., R. M.: Prediction of diurnal change in 10-h fuel stick moisture content, *Can. J. Forest Res.*, 30, 1071–1087, doi:10.1139/x00-032, 2000.
- Nelson Jr., R. M.: Water Relations of Forest Fuels, in: Forest fires, behavior and ecological effects, edited by: Johnson, E. A. and Miyanishi, K., Academic Press, San Diego, CA, 151–169, 2001.
- OpenWFM: Fire code in WRF release, Open Wildland Fire Modeling e-Community, http://www.openwfm.org/wiki/Fire_code_in_WRF_release, last access: November 2012.
- OpenWFM: Coupled WRF and SFIRE Model User's Guide, Open Wildland Fire Modeling e-Community, http://www.openwfm.org/wiki/Users_guide, last access: September 2013.

- Osher, S. and Fedkiw, R.: Level Set Methods and Dynamic Implicit Surfaces, Springer, New York, 2003.
- Peace, M., Mattner, T., and Mills, G.: The Kangaroo Island bushfires of 2007: A meteorological case study and WRF-fire simulation, Paper 3.3, Ninth Symposium on Fire and Forest Meteorology, Palm Springs, October 2011, <http://ams.confex.com/ams/9FIRE/webprogram/Paper192200.html> (retrieved: June 2012), 2011.
- Pyne, S., Andrews, P. L., and Laven, R. D.: Introduction to Wildland Fire, Wiley, New York, 1996.
- Regev, B., Amram, S., and Amit, A.: Six Hours Ahead – Predicting Wildfires in Real Time, Innovation Exchange, 16, 34–37, available at: <http://mops.gov.il/English/HomelandSecurityENG/NFServices/Pages/FirePredictionSystem.aspx> (retrieved: September 2013), 2012.
- Ritter, N. and Ruth, M.: GeoTIFF Format Specification: GeoTIFF Revision 1.0, <http://www.remotesensing.org/geotiff/spec/geotifffhome.html> (retrieved: September 2013), 2000.
- Rosenfeld, D., Fromm, M., Trentmann, J., Luderer, G., Andreae, M. O., and Servranckx, R.: The Chisholm firestorm: observed microstructure, precipitation and lightning activity of a pyro-cumulonimbus, *Atmos. Chem. Phys.*, 7, 645–659, doi:10.5194/acp-7-645-2007, 2007.
- Rothermel, R. C.: A Mathematical Model for Predicting Fire Spread in Wildland Fires, USDA Forest Service Research Paper INT-115, <http://www.treesearch.fs.fed.us/pubs/32533> (last access: October 2014), 1972.
- Schabenberger, O. and Gotway, C. A.: Statistical Methods for Spatial Data Analysis, Chapman & Hall/CRC Texts in Statistical Science, Chapman and Hall/CRC, Boca Raton, FL, 2005.
- Sethian, J. A.: Level set methods and fast marching methods, in: vol. 3 of Cambridge Monographs on Applied and Computational Mathematics, 2nd Edn., Cambridge University Press, Cambridge, 1999.
- Simpson, C. C., Sharples, J. J., Evans, J. P., and McCabe, M. F.: Large eddy simulation of atypical wildland fire spread on leeward slopes, *Int. J. Wildland Fire*, 22, 599–614, doi:10.1071/WF12072, 2013.
- Skamarock, W. C., Klemp, J. B., Dudhia, J., Gill, D. O., Barker, D. M., Duda, M. G., Huang, X.-Y., Wang, W., and Powers, J. G.: A Description of the Advanced Research WRF Version 3, NCAR Technical Note 475, http://www.mmm.ucar.edu/wrf/users/docs/arw_v3.pdf (retrieved: December 2011), 2008.
- Sullivan, A. and Ball, R.: Thermal decomposition and combustion chemistry of cellulosic biomass, *Atmos. Environ.*, 47, 133–141, doi:10.1016/j.atmosenv.2011.11.022, 2012.
- Sullivan, A. L.: A review of wildland fire spread modelling, 1990–present, 1: Physical and quasi-physical models, 2: Empirical and quasi-empirical models, 3: Mathematical analogues and simulation models, *Int. J. Wildland Fire*, 18, 1: 347–368, 2: 369–386, 3: 387–403, doi:10.1071/WF06143, doi:10.1071/WF06142, doi:10.1071/WF06144, 2009a.
- Sullivan, A. L.: A review of wildland fire spread modelling, 1990–present, 1: Physical and quasi-physical models, *Int. J. Wildland Fire*, 18, 347–368, doi:10.1071/WF06143, 2009b.
- Sullivan, A. L.: A review of wildland fire spread modelling, 1990–present 2: Empirical and quasi-empirical models, *Int. Journal of Wildland Fire*, 18, 369–386, doi:10.1071/WF06142, 2009c.
- Sullivan, A. L.: A review of wildland fire spread modelling, 1990–present 3: Mathematical analogues and simulation models, *Int. J. Wildland Fire*, 18, 387–403, doi:10.1071/WF06144, 2009d.
- USDA Forest Service: Wildland Fire Assessment System (WFAS): Dead Fuel Moisture, <http://www.wfas.net/index.php/dead-fuel-moisture-moisture--drought-38>, last access: June 2014.
- Van Wagner, C. E. and Pickett, T. L.: Equations and FORTRAN Program for the Canadian Forest Fire Weather Index System, Forestry Technical Report 33, Canadian Forestry Service, Ottawa, 1985.
- Vejmelka, M., Kochanski, A. K., and Mandel, J.: Data assimilation of dead fuel moisture observations from remote automatic weather stations, *Int. J. Wildland Fire*, arXiv:1406.4480, to appear, 2014a.
- Vejmelka, M., Kochanski, A. K., and Mandel, J.: Data assimilation of fuel moisture in WRF-SFIRE, in: Proceedings of 4th Fire Behavior and Fuels Conference, 18–22 February 2013, Raleigh, NC and 1–4 July 2013, St. Petersburg, Russia, edited by: Wade, D. D. and Fox, R. L., International Association of Wildland Fire, Missoula, MT, compiled by M. L. Robinson, 122–137, available at: http://www.iawfonline.org/4th_Fuels_Conference_Proceedings_USA-Russia.pdf, last access: July 2014b.
- Wiedinmyer, C., Akagi, S. K., Yokelson, R. J., Emmons, L. K., Al-Saadi, J. A., Orlando, J. J., and Soja, A. J.: The Fire INventory from NCAR (FINN): a high resolution global model to estimate the emissions from open burning, *Geosci. Model Dev.*, 4, 625–641, doi:10.5194/gmd-4-625-2011, 2011.